Solving boundary value problems via the Nyström method using spline Gauss rules

Ali Hashemian[a,*], Hanna Sliusarenko[a], Sara Remogna[b], Domingo Barrera[c,d], Michael Bartoň[a,e]

[a] *BCAM – Basque Center for Applied Mathematics, Alameda Mazarredo 14, 48009 Bilbao, Basque Country, Spain*
[b] *Department of Mathematics "Giuseppe Peano", University of Torino, Via Carlo Alberto 10, 10123 Torino, Italy*
[c] *Department of Applied Mathematics, University of Granada, Campus de Fuentenueva, 18071 Granada, Spain*
[d] *IMAG – Institute of Mathematics, Ventanilla 11, 18001 Granada, Spain*
[e] *Iberbasque – Basque Foundation for Sciences, María Díaz de Haro 3, 48013 Bilbao, Basque Country, Spain*

Abstract

We propose to use spline Gauss quadrature rules for solving boundary value problems (BVPs) using the Nyström method. When solving BVPs, one converts the corresponding partial differential equation inside a domain into the Fredholm integral equation of the second kind on the boundary in the sense of boundary integral equation (BIE). The Fredholm integral equation is then solved using the Nyström method, which involves a use of a particular quadrature rule, thus, converting the BIE problem to a linear system. We demonstrate this concept on the 2D Laplace problem over domains with smooth boundary as well as domains containing corners. We validate our approach on benchmark examples and the results indicate that, for a fixed number of quadrature points (i.e., the same computational effort), the spline Gauss quadratures return an approximation that is by one to two orders of magnitude more accurate compared to the solution obtained by traditional polynomial Gauss counterparts.

Keywords: Boundary value problems; Fredholm integral equation; Nyström method; spline Gauss quadratures.

1. Introduction

Boundary value problems (BVPs) are well known in engineering and science, where the given partial differential equation (PDE) is solved with respect to, e.g., Dirichlet or Neumann boundary conditions. When solving BVPs, among other approaches, one converts the corresponding PDE inside the domain into the Fredholm integral equation of the second kind on the boundary in the sense of boundary integral equation (BIE) [1–3]. The main idea is to use the fundamental solution of the governing PDE, so that approximations only occur on the domain's boundary (the solution inside the domain is then obtained via post-processing). Thus, the order of the problem is reduced by one dimension compared to, e.g., finite element analysis (FEA) [4] or isogeometric analysis (IGA) [5], where the solution approximation is performed throughout the whole domain. Another advantage is that one avoids meshing the entire domain, thus, reducing the effects of the mesh quality on the computed results.

There exist different methods addressing the numerical solution of the Fredholm integral equation of the second kind. The well-studied approaches are Galerkin (see, e.g., [3, 6, 7]) and collocation (see, e.g. [8–11]) methods. The idea of discretizing boundary integrals in the sense of finite elements, commonly known as boundary element method (BEM) [12, 13], and its extension to the IGA paradigm [14–18] are also among the well-established research in the literature. Another thematically relevant class of research are degenerate kernel methods [19, 20] allowing to approximate the integral equation with a degenerate kernel, whose solution is determined by solving a linear system of equations. Spline quasi-interpolations are known to be very useful for this purpose (c.f. [21–27] and references therein).

We consider the Nyström method [28, 29] as a classical approach for the numerical solution of Fredholm integral equations of the second kind. This method approximates the integral equation using a particular

*Corresponding author
Email address: ahashemian@bcamath.org (Ali Hashemian)

quadrature rule, thus, converting the BIE problem to a linear system of equations. The solution, obtained at quadrature points on the boundary, is then used to approximate the solution over the entire domain. In combination with other numerical methods such as FEA [30, 31] and IGA [32, 33], the Nyström method has been applied to solve problems of great practical interests with applications in, e.g., electromagnetics [34–36], fluid mechanics [37, 38] and structural analysis [39, 40].

Our research aims to point out that the way the quadrature points distribute over the boundary plays an important role in the accuracy and efficiency of the Nyström method. The classical polynomial Gaussian quadrature rules are among the well-known schemes for this purpose, yet not the only option. A survey of research on the application of different quadrature rules in the Nyström method can be found in, e.g., [41]. In this work, we propose to use spline Gauss quadrature rules for solving boundary value problems via the Nyström method. Spline Gauss rules are proved as successful alternatives to classical polynomial (discontinuous) Gauss rules when integrating high continuous functions (see, e.g., [42, 43]). When solving the Fredholm integral equation of the second kind arising from a PDE inside a 2D domain, we use a NURBS representation of the boundary curve and place the quadrature points within the knot spans of the NURBS boundary. In this context, we compare the accuracy of the solution obtained by the numerical integration using spline Gauss rules versus the solution obtained by polynomial Gauss rules. We solve the Laplace problem with Dirichlet boundary conditions on different geometries with smooth continuous boundary as well as domains containing corners. We show that when fixing the total number of quadrature points (i.e., with the same computational effort), the spline rules return an approximation that is by one to two orders of magnitude more accurate compared to the solution obtained by traditional polynomial Gauss counterparts.

The structure of the remainder of this paper is as follows. Section 2 introduces the boundary value problem and its solution via the Nyström method. Section 3 briefly recalls the notion of B-splines and Gauss quadrature rules for spline spaces. Section 4 discusses the NURBS-based boundary representation and the application of the spline Gauss rules to the solution of the BVPs via the Nyström method. Section 5 shows numerical results on three test cases, and finally, Section 6 draws some conclusions and indicates possible directions for future research.

2. Solving boundary value problems using Nyström method

Let us consider a computational domain $\Omega \subset \mathbb{R}^2$ to be the interior of a closed smooth boundary $\Gamma := \partial\Omega$. We consider the following homogeneous Dirichlet boundary value problem (see Fig. 1):

$$\text{Find } u : \Omega \to \mathbb{R} \text{ such that}$$
$$\begin{cases} \mathcal{L}u = 0\,, & \text{in } \Omega\,, \\ u = \varphi\,, & \text{on } \Gamma\,, \end{cases} \tag{2.1}$$

where $\mathcal{L}$ is the partial differential operator (e.g., $\mathcal{L} = -\Delta$ for the Laplace equation).

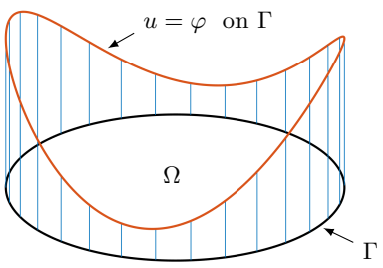

Fig. 1. Dirichlet boundary value problem: an example domain Ω, its boundary Γ, and the boundary condition φ.

2.1. Fredholm integral equation

When solving (2.1), one converts the corresponding partial differential equation inside Ω into the Fredholm integral equation of the second kind on Γ in the sense of boundary integral equation (see, e.g., [1, 44]). Let us consider $\mathbf{x}$ and $\mathbf{y}$ as points in $\mathbb{R}^2$. We assume that $\mathbf{x}$ is a point that lies either inside the domain or

on the boundary, and we further use $\widehat{\mathbf{x}}$ to emphasize the case when $\mathbf{x} \in \Gamma$. The second point $\mathbf{y}$ is assumed to lie strictly on the boundary, i.e., $\mathbf{y} \in \Gamma$. Given the solution on the boundary $\varphi(\widehat{\mathbf{x}})$, the Fredholm integral equation reads

$$\sigma(\widehat{\mathbf{x}}) - \int_\Gamma K(\widehat{\mathbf{x}}, \mathbf{y})\sigma(\mathbf{y})\, d\Gamma_{\mathbf{y}} = -2\varphi(\widehat{\mathbf{x}})\,, \qquad \widehat{\mathbf{x}}, \mathbf{y} \in \Gamma\,, \tag{2.2}$$

where σ and K are the *double-layer density* and *kernel*, respectively. Solving (2.2), one obtains the density σ on Γ and, then, the solution u of the original problem (2.1) over Ω, also called *the double-layer potential*, becomes

$$u(\mathbf{x}) = \frac{1}{2}\int_\Gamma K(\mathbf{x}, \mathbf{y})\sigma(\mathbf{y})\, d\Gamma_{\mathbf{y}}\,, \qquad \mathbf{x} \in \Omega\backslash\Gamma,\ \mathbf{y} \in \Gamma\,. \tag{2.3}$$

One obtains the kernel in (2.2) and (2.3) from the normal derivative of the *fundamental solution* $s(\mathbf{x}, \mathbf{y})$ with respect to $\mathbf{y}$, that is

$$K(\mathbf{x}, \mathbf{y}) \coloneqq 2\frac{\partial}{\partial n_{\mathbf{y}}} s(\mathbf{x}, \mathbf{y}) = 2\left\langle \mathbf{n}(\mathbf{y}), \nabla_{\mathbf{y}} s(\mathbf{x}, \mathbf{y})\right\rangle\,, \tag{2.4}$$

where $\mathbf{n}$ is the outward unit normal vector on the boundary and $\langle , \rangle$ is the Euclidean scalar product. The fundamental solution of the differential operator $\mathcal{L}$ is a function of the Euclidean norm $\|\mathbf{y} - \mathbf{x}\|$ satisfying $\mathcal{L}s = 0$ for $\mathbf{x} \neq \mathbf{y}$ (see, e.g., [1]). Herein and in the following, we restrict ourselves to the 2D Laplace equation with the following fundamental solution (for other differential equations, c.f. [1, 2, 18]):

$$s(\mathbf{x}, \mathbf{y}) = -\frac{1}{2\pi}\log\|\mathbf{y} - \mathbf{x}\|\,. \tag{2.5}$$

Thus, the double-layer kernel, which is a function of the geometry of the domain, is

$$K(\mathbf{x}, \mathbf{y}) = -\frac{1}{\pi}\frac{\langle \mathbf{n}(\mathbf{y}), \mathbf{y} - \mathbf{x}\rangle}{\|\mathbf{y} - \mathbf{x}\|^2}\,, \qquad \mathbf{x} \in \Omega,\ \mathbf{y} \in \Gamma\,. \tag{2.6}$$

2.2. Nyström method

We start from the general form of the Fredholm integral equation over a univariate domain $D \subset \mathbb{R}$, that is

$$\lambda\sigma(x) - \int_D K(x, y)\sigma(y)\, dy = \psi(x)\,, \qquad x, y \in D\,. \tag{2.7}$$

Considering an m_r-point quadrature rule, the approximation of the integral reads

$$\int_D K(x, y)\sigma(y)\, dy \approx \sum_{j=1}^{m_r} \omega_j K(x, \tau_j)\sigma_r(\tau_j)\,, \tag{2.8}$$

where τ_j and ω_j are quadrature points and weights, respectively. In here, we use subscript $r \geq 1$ to refer to the level of refinement we consider to make the quadrature rule finer and finer. We assume that for every continuous function, the numerical integrals converge to the true integral as $r \to \infty$. This implies,

$$\sup_{r\geq 1} \sum_{j=1}^{m_r} |\omega_j| < \infty\,. \tag{2.9}$$

Thus, one obtains

$$\lambda\sigma_r(x) - \sum_{j=1}^{m_r} \omega_j K(x, \tau_j)\sigma_r(\tau_j) = \psi(x)\,. \tag{2.10}$$

The Nyström method approximates the density σ_r at quadrature points, that is

$$\lambda\sigma_r(\tau_i) - \sum_{j=1}^{m_r} \omega_j K(\tau_i, \tau_j)\sigma_r(\tau_j) = \psi(\tau_i)\,, \qquad i = 1, 2, \ldots, m_r\,, \tag{2.11}$$

thus, converting the integral equation (2.7) to a $m_r \times m_r$ linear system

$$(\lambda \mathbf{I} - \mathbf{K}_r)\boldsymbol{\sigma}_r = \boldsymbol{\psi}_r \,. \tag{2.12}$$

where $\mathbf{I}$ is the unit matrix and

$$K_{ij} \coloneqq \omega_j K(\tau_i, \tau_j) \,, \tag{2.13}$$
$$\sigma_i \coloneqq \sigma_r(\tau_i) \,, \tag{2.14}$$
$$\psi_i \coloneqq \psi(\tau_i) \,. \tag{2.15}$$

Let us consider the Banach space $\mathcal{X} = C(D)$ and the operators $\mathcal{K}, \mathcal{K}_r : \mathcal{X} \to \mathcal{X}$defined as

$$\mathcal{K}\sigma(x) \coloneqq \int_D K(x,y)\sigma(y)\, dy \,, \tag{2.16}$$
$$\mathcal{K}_r\sigma_r(x) \coloneqq \sum_{j=1}^{m_r} \omega_j K(x, \tau_j)\sigma_r(\tau_j) \,, \tag{2.17}$$

associated respectively with the integral equation (2.7) and a sequence of quadrature rules of the form (2.8) such that

$$\|\mathcal{K}_r\|_\infty = \max_{x \in D} \sum_{j=1}^{m_r} |\omega_j K(x, \tau_j)| \,. \tag{2.18}$$

Regarding the convergence of the sequence σ_r provided by the Nyström method approximation, we state the following Theorem [45].

Theorem 1. Let $K(x,y)$ be a continuous kernel defined on $D \times D$, and suppose that the sequence (2.8) of quadrature rules converges for all continuous functions defined on D. Moreover, let us suppose that the integral equation (2.7) admits a unique solution for all function $\psi \in C(D)$ with $\lambda \neq 0$. Then, for r enough large, for instance $r \geq \widetilde{r}$, the operator $(\lambda - \mathcal{K}_r)^{-1}$ exists and is uniformly bounded. More precisely, there exists a constant c such that

$$\left\|(\lambda - \mathcal{K}_r)^{-1}\right\|_\infty \leq \frac{1 + \left\|(\lambda - \mathcal{K})^{-1}\right\|_\infty \|\mathcal{K}_r\|_\infty}{|\lambda| - \left\|(\lambda - \mathcal{K})^{-1}\right\|_\infty \|(\mathcal{K} - \mathcal{K}_r)\mathcal{K}_r\|_\infty} \leq c \,, \qquad r \geq \widetilde{r} \,. \tag{2.19}$$

Furthermore, for the solutions of equations $(\lambda - \mathcal{K})\sigma = \psi$ and $(\lambda - \mathcal{K}_r)\sigma_r = \psi$, it holds

$$\|\sigma - \sigma_r\|_\infty \leq \left\|(\lambda - \mathcal{K}_r)^{-1}\right\|_\infty \|(\mathcal{K} - \mathcal{K}_r)\sigma\|_\infty \leq c\, \|(\mathcal{K} - \mathcal{K}_r)\sigma\|_\infty \,, \qquad r \geq \widetilde{r} \,. \tag{2.20}$$

We recall that the sequences of Gaussian quadrature rules (considered in this work) are convergent for all continuous functions because they have positive weights (see, e.g., [46, Theorem 3] and [47, p. 130]).

Remark 1. If there is no danger of confusion, we omit the subscript r for the number of quadrature points m_r and will write simply m. Our limiting process, for $r \to \infty$, will be realized in terms of refinement of the domain D into N subdomains, each corresponding to an m-point quadrature rule. The weighted kernel matrix in (2.13) is then evaluated *globally* for the entire D, i.e., for $i, j = 1, 2, \ldots, M$, where $M \coloneqq mN$.

The application of the Nyström method to multidimensional PDEs is analogous. Considering (2.2), we set $\lambda = 1$ and $\psi = -2\varphi$. In the 2D case, particularly, we consider the quadrature points along the boundary curve Γ. Thus, when integrating (2.2), we need to perform a curve *rectification* to transfer from $\Gamma \subset \mathbb{R}^2$ to the univariate domain $D \subset \mathbb{R}$. For this purpose, we consider a NURBS representation of the boundary that maps D onto Γ (see Section 4.3). Once we compute densities on the boundary from (2.12), we obtain the point-wise solution u at each arbitrary point $\mathbf{x}$ inside the domain from (2.3).

Remark 2. For every $\mathbf{x} \in \Omega \backslash \Gamma$, the kernel is non-singular. For boundary points $\widehat{\mathbf{x}} \in \Gamma$, however, singularity may occur in the limit when $\widehat{\mathbf{x}} \to \mathbf{y}$. At such points, when Γ is at least C^2 continuous, we have no singularities

as the kernel expresses the (scaled) curvature of the boundary curve (see Fig. 2). More precisely, one obtains the kernel as follows [1]:

$$\lim_{\widehat{\mathbf{x}}\to\mathbf{y}} K(\widehat{\mathbf{x}},\mathbf{y}) = -\frac{1}{2\pi}\kappa(\mathbf{y})\,, \tag{2.21}$$

where $\kappa(\mathbf{y})$ denotes the curvature of Γ at $\mathbf{y}$. For C^0 boundaries, the singularity occurs at the vicinity of corners, where one observes a discontinuity of the normal vector. For such occasions, the Strain's locally correction algorithm can be used. We refer the readers to [32, 48, 49] for more details.

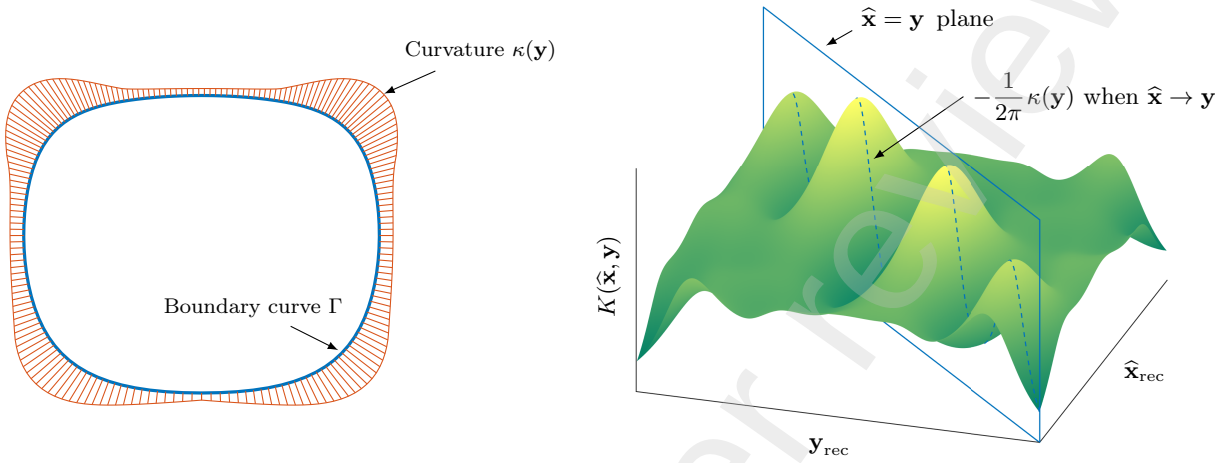

Fig. 2. Left: A general domain represented by its C^2 boundary curve Γ. We show the curvature distribution over the boundary. Right: 2D representation of the kernel $K(\widehat{\mathbf{x}},\mathbf{y})$ on the boundary. When $\widehat{\mathbf{x}}\to\mathbf{y}$, the kernel is equal to the scaled curvature of the boundary curve (dashed line). For better representation, we plot the kernel against $\widehat{\mathbf{x}}_{\text{rec}}$ and $\mathbf{y}_{\text{rec}}$ as the rectified values of $\widehat{\mathbf{x}}$ and $\mathbf{y}$, respectively (see Section 4.3).

3. Spline Gauss quadrature rules

3.1. B-spline spaces: preliminaries

We use B-spline spaces both for spline Gauss quadrature rules and for the NURBS representation of the domain's boundary (see Section 4). We define the spline space $\mathcal{S}^N_{p,\mathbf{c}}$ as the set of p-th degree B-spline basis functions spanned over the knot sequence

$$\Xi := \{\underbrace{\xi_0,\ldots,\xi_0}_{\mu_0},\underbrace{\xi_1,\ldots,\xi_1}_{\mu_1},\ldots,\underbrace{\xi_N,\ldots,\xi_N}_{\mu_N}\} = \{\Xi_0,\Xi_1,\ldots,\Xi_{n+p+1}\}, \tag{3.1}$$

where N knot spans are characterized by non-repeating knots ξ_k, $k=0,1,\ldots,N$. We denote knot *multiplicities* by μ_k such that $1\le\mu_k\le p+1$ and $\sum_{k=0}^{N}\mu_k = n+p+2$ where $n+1$ is the dimension of the spline space. We also introduce $\mathbf{c}$ as the continuity vector whose components are $c_k := p-\mu_k$. For any arbitrary parameter $\xi_0\le\xi\le\xi_N$, we obtain the i-th basis function $B_{i,p}(\xi)$, $i=0,1,\ldots,n$, by the Cox–De Boor recursion as follows [50]:

$$B_{i,0}(\xi) = \begin{cases} 1\,, & \Xi_i\le\xi<\Xi_{i+1}\,,\\ 0\,, & \text{otherwise}\,,\end{cases} \tag{3.2}$$

$$B_{i,p}(\xi) = \frac{\xi-\Xi_i}{\Xi_{i+p}-\Xi_i}B_{i,p-1}(\xi) + \frac{\Xi_{i+p+1}-\xi}{\Xi_{i+p+1}-\Xi_{i+1}}B_{i+1,p-1}(\xi)\,, \tag{3.3}$$

where its l-th order derivative ($l=1,2,\ldots,p$) is given by:

$$B^{(l)}_{i,p}(\xi) = p\left(\frac{B^{(l-1)}_{i,p-1}(\xi)}{\Xi_{i+p}-\Xi_i} - \frac{B^{(l-1)}_{i+1,p-1}(\xi)}{\Xi_{i+p+1}-\Xi_{i+1}}\right). \tag{3.4}$$

When evaluating basis functions and their derivatives at a desired ξ, we find the corresponding nonzero knot span in (3.2) and efficiently evaluate (3.3) and (3.4) avoiding any division by zero in dealing with repetitive knots. More details are given in [50, Algorithms A2.1–A2.3] and [51, Algorithms A1 and A2].

3.2. Spline vs. polynomial Gauss quadrature rules

Let D be our univariate integration domain and $T \subset D$ be a set of m quadrature points τ_j, $j = 1, 2, \ldots, m$, inside D. We consider the m-point quadrature rule

$$\int_D f(x)\, dx \approx \sum_{j=1}^{m} \omega_j f(\tau_j)\,, \qquad \tau_j \in T \subset D\,, \tag{3.5}$$

that approximates the integral of $f(x)$ over D and converges to the exact integral as $m \to \infty$. Typically, equation (3.5) is not just an approximation, but it is exact for a certain linear space of functions. A rule is said to be Gaussian if m is the minimum required number of quadrature points at which f is evaluated, while guaranteeing the exactness of the integration.

Remark 3. When integrating polynomial functions, the optimal rule in terms of the number of quadrature points is known to be the classical Gauss quadrature rule [52] with the order of exactness $2m - 1$, that is, a set of m evaluations are needed to exactly integrate any polynomial of degree at most $2m - 1$ over D.

Let the integration domain consist of N *elements* $D_k \subset D$, $k = 1, 2, \ldots, N$, the element-wise integration over D using the classical polynomial Gauss quadrature rule entails an m-point rule within *each* element. This is equal to the discontinuous spline Gauss rule when using a spline space with C^{-1} continuity at all elements interfaces. However, when integrating continuous functions, it is computationally inefficient to use polynomial Gauss rules on every element. Instead, we use high-continuity spline Gauss rules, thus performing the integration over *macroelements*. In this manner, every macroelement consists of a set of elements corresponding to knot spans of the respective spline space and the quadrature points are distributed over the macroelement. The existence and uniqueness of Gaussian quadrature rules for spline spaces of *uniform* continuity has been studied in [53] and [54, Theorem 3.4], respectively (herein by uniform we refer to spaces with equal multiplicities at all interior knots). Let us consider the spline space $\mathcal{S}^{\widetilde{N}}_{\widetilde{p},\widetilde{c}}$ of $\widetilde{p}$-th degree basis functions spanned over a macroelement of $\widetilde{N}$ uniform elements with a uniform continuity $\widetilde{c} \coloneqq \widetilde{p} - \widetilde{\mu}$, where $\widetilde{\mu}_1 = \widetilde{\mu}_2 = \widetilde{\mu}_{\widetilde{N}-1} = \widetilde{\mu}$ (we use $\widetilde{\ }$ to distinguish this spline space from the space we employ for the NURBS representation of the boundary in Section 4). For spline spaces, there always exists a Gaussian quadrature rule [54] where the number of necessary evaluations m is given by:

$$\widetilde{p} + \iota + 1 = 2m\,, \tag{3.6}$$

noting that $\iota \coloneqq \big(\widetilde{N} - 1\big)\widetilde{\mu}$ is the total number of interior knots, including their multiplicities. This fact is in accordance with the dimension of the spline space, which is the maximum number of basis functions to be integrated exactly by only half the number of quadrature points. If $\widetilde{p} \ll \iota$, then $m \approx \iota/2$, denoting that in the limit, when $\widetilde{N} \to \infty$, the spline rules converge to the half-point rules of Hughes et al. [55], which are exact and Gaussian over the domain.

We use the polynomial homotopy continuation (PHC), a numerical scheme for solving polynomial systems of equations [56], to generate Gaussian quadrature rules for spline spaces of higher continuities (as it has been used in, e.g., [42, 43, 57]). The main advantage of using such spaces is that we can integrate using Gaussian rules with lower number of quadratures (i.e., evaluations), while preserving the same order of exactness (see [58]). In particular, to generate a Gaussian rule in a *target* spline space, we built an associated *source* space with known Gaussian quadratures (e.g., a union of polynomial Gauss rules) and transform the rule from the source space to the target space, while preserving the optimality. The exactness of the quadrature rule is formulated as a polynomial system where the quadrature points and weights are zeros of this system. Using the homotopy continuation concept, the source space is continuously deformed by changing the source knot sequence towards the target configuration and the quadrature rule gets updated numerically by tracing the unique root of the continuously modified piecewise polynomial system. We omit details for the sake of brevity (see, e.g., [42] for more details). Fig. 3 shows two different cubic spaces with the same order of exactness spanned over the same number of elements. In particular, Fig. 3a represents the maximum-continuity spline space $\mathcal{S}^9_{3,2}$ (spanned over a macroelement of size $\widetilde{N} = 9$) that needs only 6 quadrature points for all elements according to (3.6), while Fig. 3b shows the discontinuous space $\mathcal{S}^9_{3,-1}$ that needs 18

quadrature points. Using the latter space is equivalent to the element-wise integration by the classical polynomial Gauss rule with two quadrature points within every element. From the computational point of view, with the same order of exactness, the spline rule is more efficient than the polynomial rule because it has a lower number of quadrature points (i.e., lower evaluations).

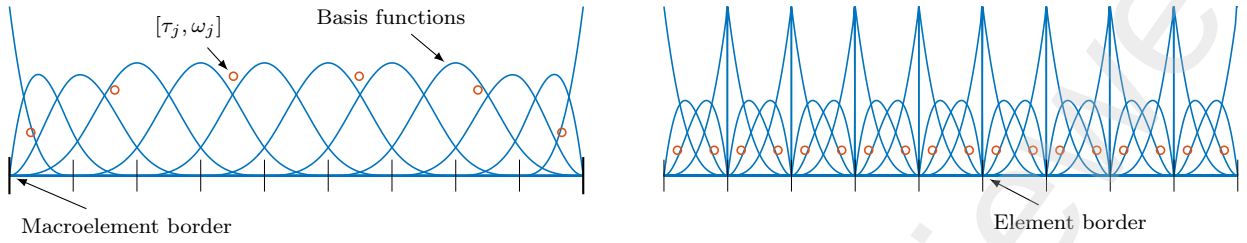

(a) Maximum-continuity space $\mathcal{S}^9_{3,2}$ (b) Discontinuous (polynomial) space $\mathcal{S}^9_{3,-1}$

Fig. 3. Two different cubic spaces: (a) $\mathcal{S}^9_{3,2}$ and (b) $\mathcal{S}^9_{3,-1}$, both spanned over 9 elements. The quadrature points τ_j and respective weights ω_j are shown with red circles. The spline space in (a) represents a 6-point rule for the entire domain and obtains the same order of exactness when compared to the discontinuous space in (b) that needs 18 quadrature points (equivalent to the 2-point element-wise polynomial Gauss rule).

4. NURBS-based boundary representation

4.1. NURBS curve: a short review

Given the parametric domain $D \subset \mathbb{R}$, we represent the boundary curve $\Gamma \subset \mathbb{R}^2$ as a p-th degree piecewise continuous NURBS curve $\mathbf{C} : D \to \mathbb{R}^2$ with $n+1$ control points $\mathbf{P}_i \in \mathbb{R}^2$ and corresponding non-negative weights $w_i \in \mathbb{R}^+$, $i = 0, 1, \ldots, n$. Considering the control point $\mathbf{P}_i = (P_{i,x}, P_{i,y})$, we use the *homogeneous coordinates* and introduce $\mathbf{P}^w_i := (w_i P_{i,x}, w_i P_{i,y}, w_i)$ to represent the boundary by a (non-rational) B-spline curve in the homogeneous coordinates as follows [50]:

$$\mathbf{C}^w(\xi) = \sum_{i=0}^{n} B_{i,p}(\xi)\mathbf{P}^w_i \,. \tag{4.1}$$

Defining

$$\mathbf{A}(\xi) := \big(C^w_x(\xi), C^w_y(\xi)\big) \,, \tag{4.2}$$

$$W(\xi) := \sum_{i=0}^{n} B_{i,p}(\xi) w_i \,, \tag{4.3}$$

one writes $\mathbf{C}^w(\xi) = \big(\mathbf{A}(\xi), W(\xi)\big)$. Thus, the NURBS representation of the boundary curve Γ is

$$\mathbf{C}(\xi) = \frac{\mathbf{A}(\xi)}{W(\xi)} \,, \tag{4.4}$$

and its l-th order derivative reads

$$\mathbf{C}^{(l)}(\xi) = \frac{\mathbf{A}^{(l)}(\xi) - \sum_{i=1}^{l} \binom{l}{i} W^{(i)}(\xi)\mathbf{C}^{(l-i)}(\xi)}{W(\xi)} \,. \tag{4.5}$$

where we obtain $\mathbf{A}^{(l)}(\xi)$ and $W^{(l)}(\xi)$ from

$$\mathbf{C}^{w\,(l)}(\xi) = \sum_{i=0}^{n} B^{(l)}_{i,p}(\xi)\mathbf{P}^w_i = \big(\mathbf{A}^{(l)}(\xi), W^{(l)}(\xi)\big) \,. \tag{4.6}$$

4.2. Continuity, corner modeling, and unclamping

A piecewise NURBS curve of degree p with a knot sequence in the form of (3.1) is $C^{p-\mu_k}$ continuous at ξ_k. If $\mu_0 = \mu_N = p+1$, the curve is *clamped* at both ends (Figs. 4a–4c). If all *interior* knots are *single*, the curve has the maximum continuity everywhere (see, e.g., Fig. 4a). In the same manner, if the multiplicity

of an interior knot equals to p, the curve is C^0 at that knot, allowing us to model corners. The mapped position of such multiple knot on the curve coincides with the respective control point (Fig. 4b). The boundary curve Γ in the Fredholm integral equation (2.2) is closed and *periodic*. To have a closed boundary curve, we may simply set $\mathbf{P}_0 = \mathbf{P}_n$ (see Fig. 4c), while to maintain the periodicity, we *unclamp* the curve. The unclamping process starts from a closed curve and proceed with changing the first and last p knots, and first and last $p-1$ control points and weights (Fig. 4d). More details on different unclamping methods are given in [50, Algorithm A12.1].

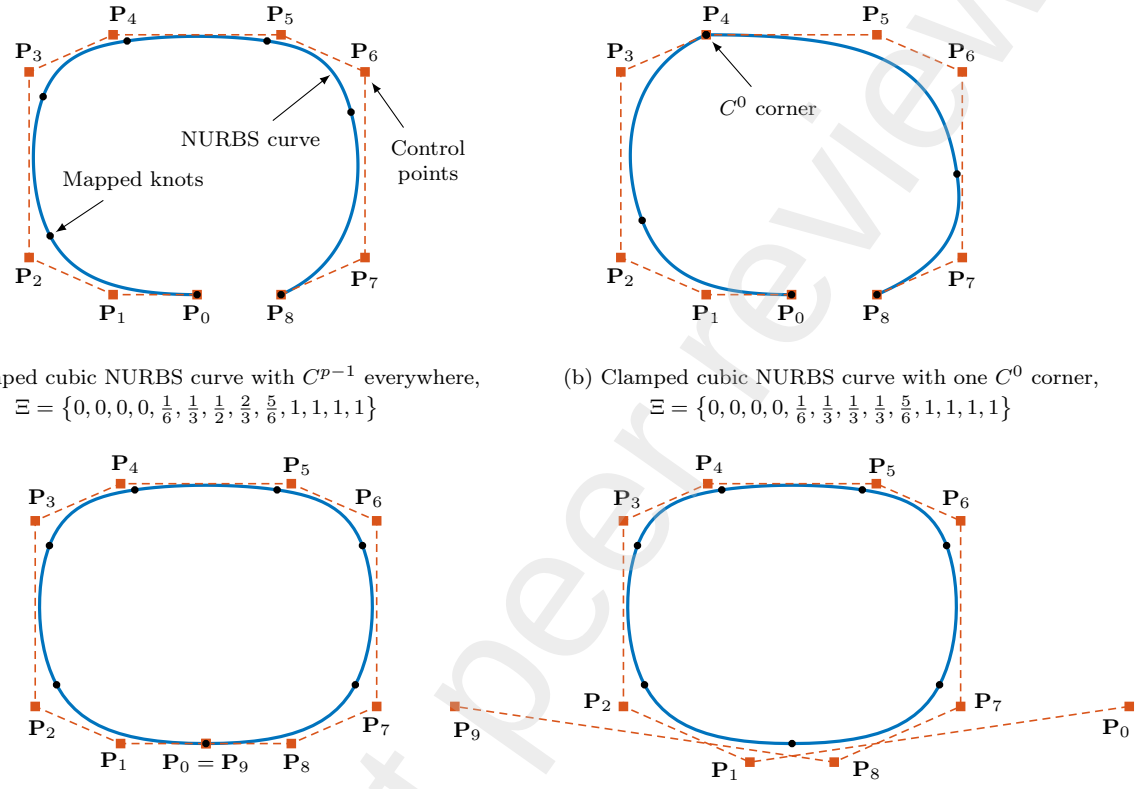

(a) Clamped cubic NURBS curve with C^{p-1} everywhere, $\Xi = \{0,0,0,0,\frac{1}{6},\frac{1}{3},\frac{1}{2},\frac{2}{3},\frac{5}{6},1,1,1,1\}$

(b) Clamped cubic NURBS curve with one C^0 corner, $\Xi = \{0,0,0,0,\frac{1}{6},\frac{1}{3},\frac{1}{3},\frac{1}{3},\frac{5}{6},1,1,1,1\}$

(c) Closed cubic NURBS curve, $\Xi = \{0,0,0,0,\frac{1}{7},\frac{2}{7},\frac{3}{7},\frac{4}{7},\frac{5}{7},\frac{6}{7},1,1,1,1\}$

(d) Periodic form of the cubic NURBS curve of part (c), $\Xi = \{\frac{-3}{7},\frac{-2}{7},\frac{-1}{7},0,\frac{1}{7},\frac{2}{7},\frac{3}{7},\frac{4}{7},\frac{5}{7},\frac{6}{7},1,\frac{8}{7},\frac{9}{7},\frac{10}{7}\}$

Fig. 4. Some possible representations of a cubic NURBS curve with 9 (fixed) control points and different knot sequences over $D : [0,1]$. In (a), (b) and (c), the curve is clamped at both ends. In (c), a new control point is wrapped on the first one to close the curve. (d) shows the unclamped version of (c), where the first and last two control points and weights are updated. Although it forces the knot sequence to violate $[0,1]$, we still consider $\xi \in [0,1]$ in (4.1) to obtain the desired boundary curve.

4.3. Application to BVPs and Nyström method

We consider boundary curve Γ as a bijective and differentiable mapping of the parameter space $D \subset \mathbb{R}$ onto $\mathbb{R}^2$, i.e., $\Gamma := \{\mathbf{y} = \mathbf{C}(\xi) : \xi \in D \to \mathbb{R}^2\}$. We then compute the boundary integrals in (2.2) and (2.3) over the parametric domain D. Thus, we write

$$d\Gamma_{\mathbf{y}} = \left\|\mathbf{C}'(\xi)\right\| d\xi\,, \tag{4.7}$$

$$\mathbf{n}(\xi) = \frac{\left[C'_y(\xi), -C'_x(\xi)\right]}{\left\|\mathbf{C}'(\xi)\right\|}\,, \tag{4.8}$$

$$\kappa(\xi) = \frac{\left\|\mathbf{C}'(\xi) \times \mathbf{C}''(\xi)\right\|}{\left\|\mathbf{C}'(\xi)\right\|^3}\,. \tag{4.9}$$

Further, we consider the boundary Γ as the union of N segments Γ_k, $k = 1, 2, \ldots, N$, being the mappings of nonzero knot spans $D_k := [\xi_{k-1}, \xi_k] \subset D$. Let $\xi \in D_k$ and $\zeta \in D$ be arbitrary parameters, we write $\mathbf{y}(\xi) = \mathbf{C}(\xi)$ and $\widehat{\mathbf{x}}(\zeta) = \mathbf{C}(\zeta)$. Then, we obtain the kernel integral in the sense of Remark 1 as follows:

$$\int_{\Gamma} K(\widehat{\mathbf{x}},\mathbf{y})\sigma(\mathbf{y})\,d\Gamma_{\mathbf{y}} = \sum_{k=1}^{N}\int_{D_k} K\big(\widehat{\mathbf{x}}(\zeta),\mathbf{y}(\xi)\big)\sigma\big(\mathbf{y}(\xi)\big)\|\mathbf{y}'(\xi)\|\,d\xi\,, \qquad \zeta\in D\,,\xi\in D_k\,. \tag{4.10}$$

The second kind Fredholm integral equation (2.2) is then

$$\sigma\big(\widehat{\mathbf{x}}(\zeta)\big) - \sum_{k=1}^{N}\int_{D_k} K\big(\widehat{\mathbf{x}}(\zeta),\mathbf{y}(\xi)\big)\sigma\big(\mathbf{y}(\xi)\big)\|\mathbf{y}'(\xi)\|\,d\xi = -2\varphi\big(\widehat{\mathbf{x}}(\zeta)\big)\,, \qquad \zeta\in D\,,\xi\in D_k\,. \tag{4.11}$$

We apply the Nyström method to (4.11), thus selecting the evaluation parameters ξ and ζ at quadrature points. Let us consider $T_k \subset D_k$ as the set of quadrature points $\tau_{j,k}$, $j=1,2,\ldots,m$, corresponding to an m-point quadrature rule inside D_k, and $T \coloneqq T_1\cup T_2\cup\ldots\cup T_N$. We write the Nyström approximation of the integral equation (4.11) as follows:

$$\sigma\big(\widehat{\mathbf{x}}(\tau_i)\big) - \sum_{k=1}^{N}\sum_{j=1}^{m}\omega_{j,k}K\big(\widehat{\mathbf{x}}(\tau_i),\mathbf{y}(\tau_{j,k})\big)\sigma\big(\mathbf{y}(\tau_{j,k})\big)\|\mathbf{y}'(\tau_{j,k})\| = -2\varphi\big(\widehat{\mathbf{x}}(\tau_i)\big)\,, \quad \tau_i\in T, \tau_{j,k}\in T_k. \tag{4.12}$$

In order to qualitatively compare the results produced by the polynomial and spline Gauss rules, we fix the *total* number of quadrature points M for both rules (since it corresponds to the computational effort of the numerical integration) and find the required N and m in (4.12) for each method accordingly. We recall that for the spline rule, we perform the integration macroelement-wise. Starting from a NURBS boundary with N segments, we assume every nonzero knot span $[\xi_{k-1},\xi_k]$, $k=1,2,\ldots,N$, of Γ as one macroelement associated with the spline space $\mathcal{S}^{\widetilde{N}}_{\widetilde{p},\widetilde{c}}$ with the same $\widetilde{p}$, $\widetilde{c}$ and $\widetilde{N}$ for all macroelements. Thus, without loss of generality, for the spline Gauss rule, we write $N = N_{\text{me}}$ where N_{me} is the number of macroelements. The number of quadrature points of the spline rule m_{s} is governed by (3.6). For the polynomial Gauss rule with an m_{p}-point element-wise integration, we use the following formula to obtain the appropriate number of elements N_{p} such that we have the same total quadrature points (M) as the spline rule:

$$M \coloneqq N_{\text{me}}m_{\text{s}} = N_{\text{p}}m_{\text{p}}\,. \tag{4.13}$$

We note that based on the exactness criterion of polynomial Gauss rules (Remark 3), we compare an m_{p}-point polynomial rule with a spline rule of degree $\widetilde{p} = 2m_{\text{p}}-1$. When fixing M, we observe a higher flexibility of the continuous spline space than the (discontinuous) polynomial alternative. This is because the spline space spans over $N_{\text{me}}\widetilde{N}$ elements, while its polynomial counterpart spans over $N_{\text{p}} < N_{\text{me}}\widetilde{N}$ elements (see Fig. 5). This reflects lower approximation errors when using spline Gauss rules while preserving the same computational effort (see [58]).

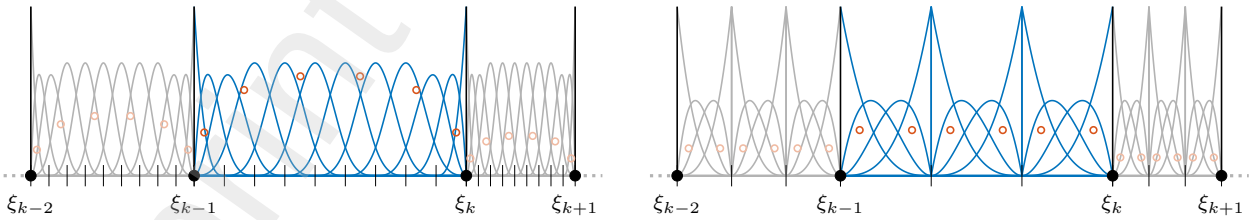

(a) Spline Gauss quadratures with $\mathcal{S}^{9}_{3,2}$ for every macroelement

(b) Polynomial Gauss quadratures with a 2-point rule for every element

Fig. 5. Spline vs. polynomial Gauss quadratures over the non-uniform knot spans of an arbitrary NURBS boundary (we highlight the k-th span for better visualization). When fixing the total number of quadrature points (in here, six points at every knot span), the spline Gauss rule in (a) corresponds to a higher number elements compared to its polynomial counterpart in (b), thus resulting in a more accurate integration with the same computational efficiency.

5. Numerical results

We verify the presented methodology by three case studies. Before reporting the results, some important notes need to be considered:

- To investigate the numerical accuracy of the spline and polynomial Gauss quadrature rules, we set $m_{\mathrm{p}} = 2, 3$ and compare the corresponding 2- and 3-point element-wise polynomial rules with the spline rules of the cubic $\mathcal{S}^{39}_{3,2}$ and quintic $\mathcal{S}^{37}_{5,4}$ spaces, respectively. These spline spaces both contain 21 quadrature points at each macroelement. Table 1 represents the quadrature points τ_j and weights ω_j of mentioned spaces in $[0, 1]$. The corresponding polynomial Gauss counterparts are also tabulated. We note that it is possible to experiment with different number of macroelements, or even higher degrees, (see [42, 43, 57, 58] for more spaces). One could even compute the Gaussian rules recursively, deriving a rule for the whole domain, not just a single block (c.f [59]). However, such a rule is of reduced continuity (e.g., quintic C^1 splines) and is not expected to perform much better in terms of the number of quadrature vs. accuracy.
- In all examples, we construct either spline or polynomial quadrature rules within the nonzero knot spans of the parametric domain of the NURBS boundary curve. To improve the numerical accuracy of the Nyström method, we follow the h-refinement idea in FEA and IGA (see [32]). Thus, we enrich the knot sequence of the original NURBS geometry and increase the total number of quadrature points M. Depending the domain's geometry, we may employ the *grading* algorithm to insert knots in appropriate places [32, 60, 61], thus, reaching a better approximation of the solution near corners.
- We study the maximum point-wise error of the Nyström approximation when doubling the number of quadrature points at every refinement level. Let e_i be the maximum point-wise error at the i-th level, we obtain the numerical convergence order as

$$\mathcal{NCO}_i \coloneqq \log_2\left(\frac{e_{i-1}}{e_i}\right), \tag{5.1}$$

where the theoretical rate is $\widetilde{p}+1$ (see, e.g., [3]).

Table 1. Quadrature points and weights of two spline Gauss rules in $[0, 1]$, characterized by cubic $\mathcal{S}^{39}_{3,2}$ and quintic $\mathcal{S}^{37}_{5,4}$ spline spaces (see [42, 43, 57, 58] for more spaces). Thanks to the symmetry property of the spline spaces, only the first 11 points and weights are reported. The corresponding points and weights of the 2- and 3-point polynomial Gauss rules are also tabulated.

j	τ_j	ω_j	τ_j	ω_j
	$\mathcal{S}^{39}_{3,2}$ (C^2 cubic spline Gauss rule with $\widetilde{N}=39$)		$\mathcal{S}^{37}_{5,4}$ (C^4 quintic spline Gauss rule with $\widetilde{N}=37$)	
1	0.0086022074347388	0.0218455595269063	0.0057434073557755	0.0148734239383008
2	0.0423693959303822	0.0433045545577068	0.0306123827542799	0.0343754550330581
3	0.0901289847662636	0.0503213631747089	0.0722191092726851	0.0473488367225914
4	0.1410569521267253	0.0512021143533085	0.1226181175788537	0.0524452767387078
5	0.1923101843694322	0.0512756766459810	0.1758677573121231	0.0537340667590496
6	0.2435899416018961	0.0512815446928528	0.2297657904899482	0.0539935956159231
7	0.2948718106031808	0.0512820110347811	0.2837905183402830	0.0540427493680052
8	0.3461538474036372	0.0512820480845737	0.3378390942637572	0.0540519443566724
9	0.3974358975351839	0.0512820510280155	0.3918921259881264	0.0540536600406546
10	0.4487179487257872	0.0512820512617426	0.4459459881438810	0.0540539780926602
11	0.5000000000000000	0.0512820512788446	0.5000000000000000	0.0540540266687536
	2-point element-wise polynomial Gauss rule		3-point element-wise polynomial Gauss rule	
1	0.2113248654051871	0.5000000000000000	0.1127016653792583	0.2777777777777778
2	0.7886751345948129	0.5000000000000000	0.5000000000000000	0.4444444444444444
3	–	–	0.8872983346207417	0.2777777777777778

5.1. Laplace problem on a square domain

We consider the benchmark 2D Laplace problem on a unit square with a sinusoidal boundary condition along one edge while the other three edges have homogeneous boundary conditions (see, e.g., [62, 63]):

Find $u : \Omega \to \mathbb{R}$ with $\Omega \coloneqq [0, 1]^2$, such that

$$\begin{cases} \Delta u(x, y) = 0\,, & \text{in } \Omega\,, \\ u(x, 0) = \sin \pi x\,, \\ u(x, 1) = u(0, y) = u(1, y) = 0\,. \end{cases} \tag{5.2}$$

The analytical solution of (5.2), obtained by separation of variables, is:

$$u(x, y) = (\cosh \pi y - \coth \pi \sinh \pi y) \sin \pi x \,. \tag{5.3}$$

Fig. 6 shows a NURBS representation of the boundary characterized by five control points $\mathbf{P}_0$ to $\mathbf{P}_4$ and linear B-spline basis functions (i.e., $p = 1$). The analytical solution over the domain is also depicted in the figure.

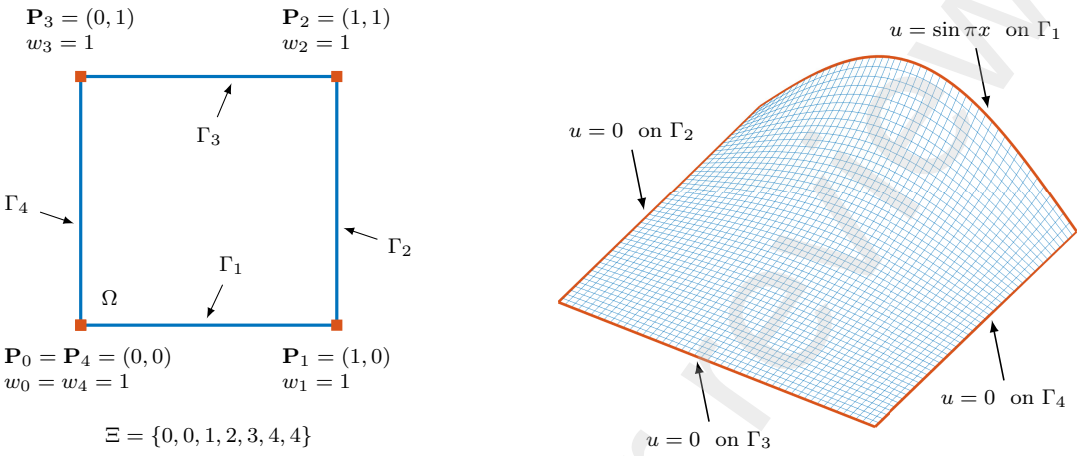

Fig. 6. Left: NURBS representation of the square boundary of problem (5.2): control points, weights and knot sequence before unclamping (for better visualization, we name different parts of the boundary as $\Gamma_1, \ldots, \Gamma_4$). Right: analytical solution over the domain.

Fig. 7 shows the maximum point-wise error of the Nyström approximation of the solution of the Dirichlet boundary value problem (5.2) when doubling the number of quadrature points at every refinement step. To do this, we compute the approximation error at different points distributed through the square domain by comparing the approximate solution obtained by (2.3) with the analytical expression (5.3). We compare the solutions when using the polynomial and spline Gauss rules and integrating with the same total number of quadrature points M. The results indicate that the spline rule is at least one order of magnitude more accurate than the polynomial rule. Additionally, the numerical convergence order is very close to the

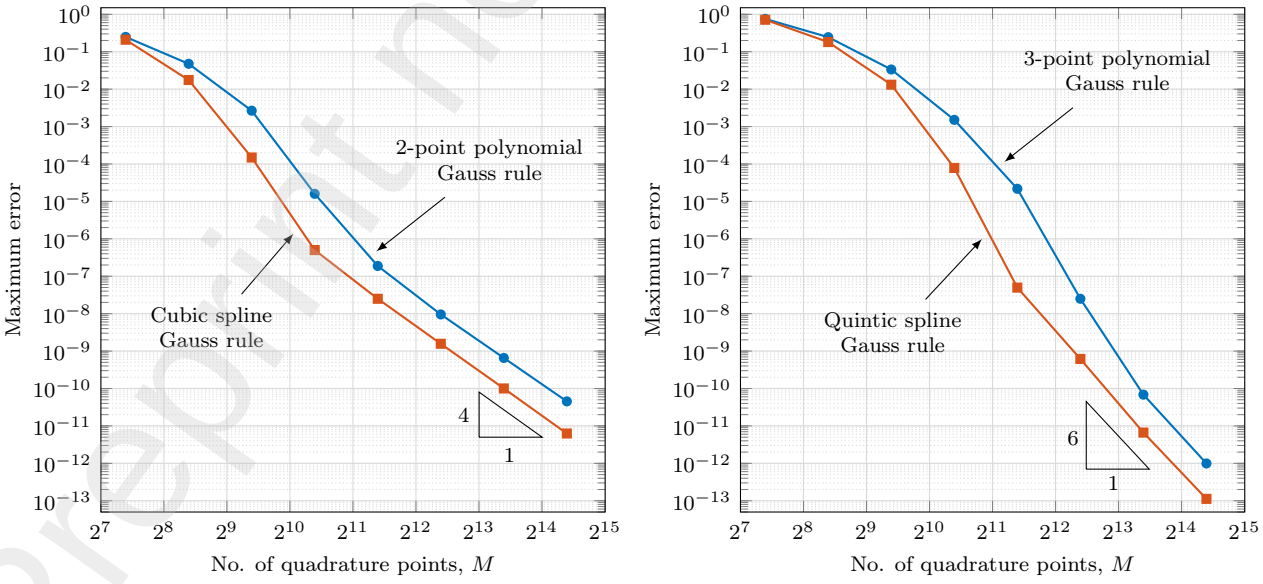

(a) $\widetilde{p} = 3$ (b) $\widetilde{p} = 5$

Fig. 7. Maximum point-wise error of the Nyström approximation of the solution of (5.2) over the square domain. (a) Gauss cubic spline vs. Gauss 2-point polynomial rule. (b) Gauss quintic spline vs. Gauss 3-point polynomial rule. The respective numerical convergence orders are shown by the triangles.

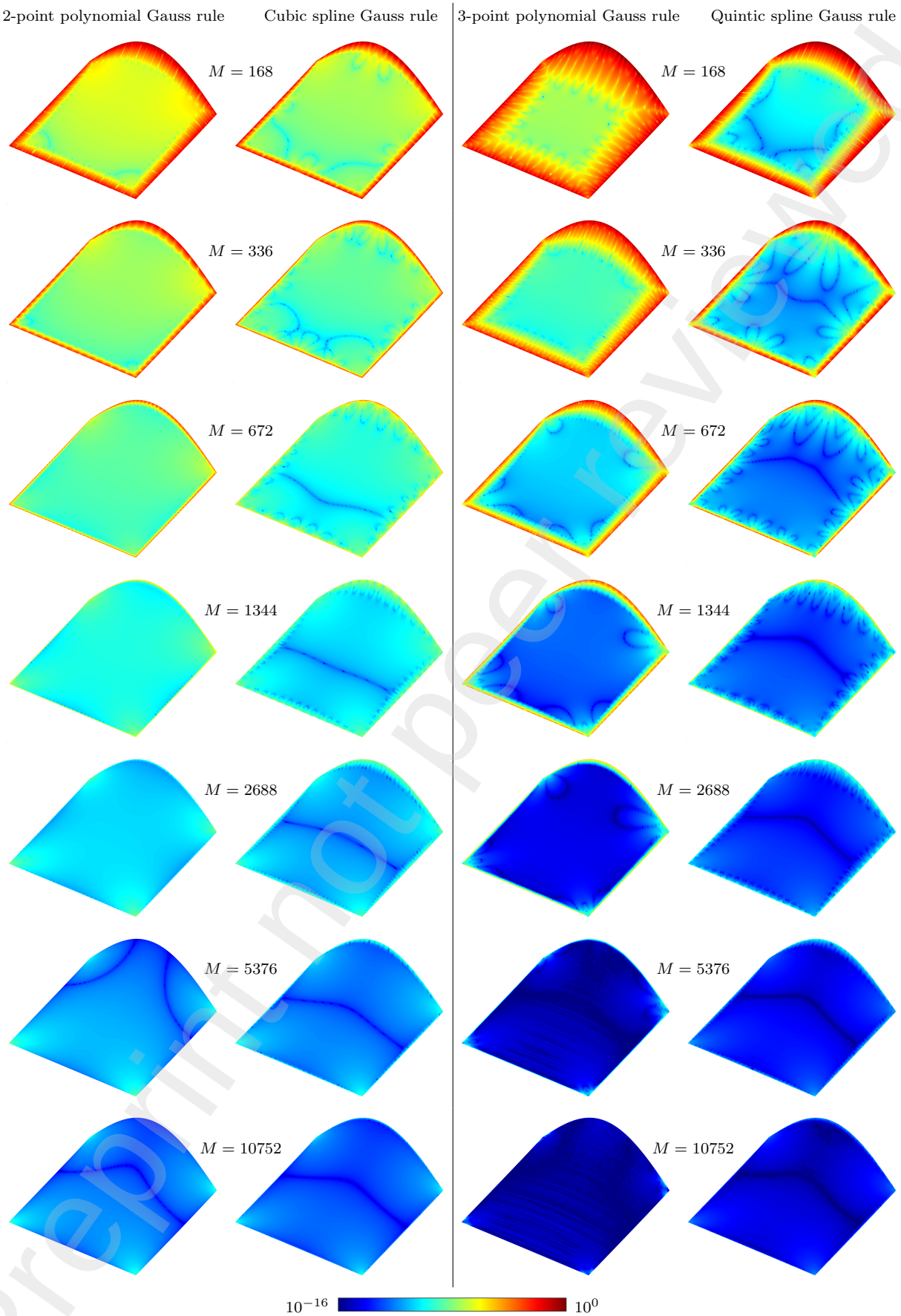

Fig. 8. Error distributions over the square domain at different refinement levels of the Nyström approximation using M quadrature points. We compare 2- and 3-point polynomial Gauss rules with their cubic and quintic spline counterparts, respectively. We place the error plots over the analytical solution surface and color-code it by the approximation error.

theoretical one, that is, $\mathcal{NCO} \approx \widetilde{p}+1$. It is clear that for a higher $\widetilde{p}$, we observe a better approximation. It could be thought of as equal to the p-refinement idea in FEA and IGA. In order to visualize how the approximation error distributes throughout the domain, we represent the error plots over the square domain in Fig. 8. The results indicate that the spline Gauss quadrature rule has a better approximation quality at all refinement steps.

5.2. Laplace problem on a unit disk

We seek the solution of the Dirichlet boundary value problem of the Laplace equation on a unit disk [64]:

$$\text{Find } u : \Omega \to \mathbb{R} \text{ with } \Omega \coloneqq \big\{(r,\theta) : r \in [0,1], \theta \in [0,2\pi]\big\}, \text{ such that}$$
$$\begin{cases} \Delta u = 0\,, & \text{in } \Omega\,, \\ u = \cos 2\theta\,, & \text{on } \Gamma\,. \end{cases} \tag{5.4}$$

The analytical solution of (5.4) in the polar coordinate system is:

$$u(r,\theta) = r^2 \cos 2\theta\,. \tag{5.5}$$

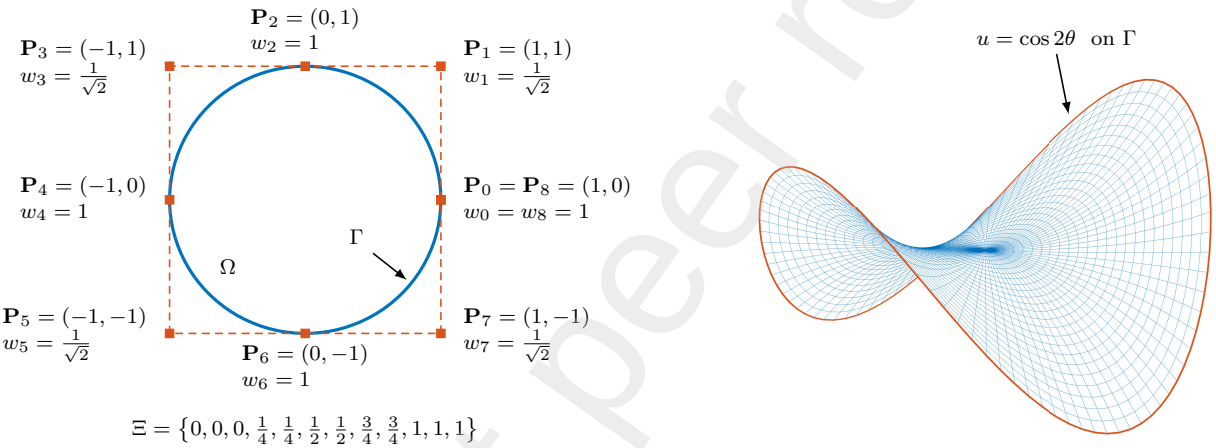

Fig. 9. Left: NURBS representation of the circular boundary of the problem (5.4): control points, weights and knot sequence (before unclamping). Right: analytical solution over the domain.

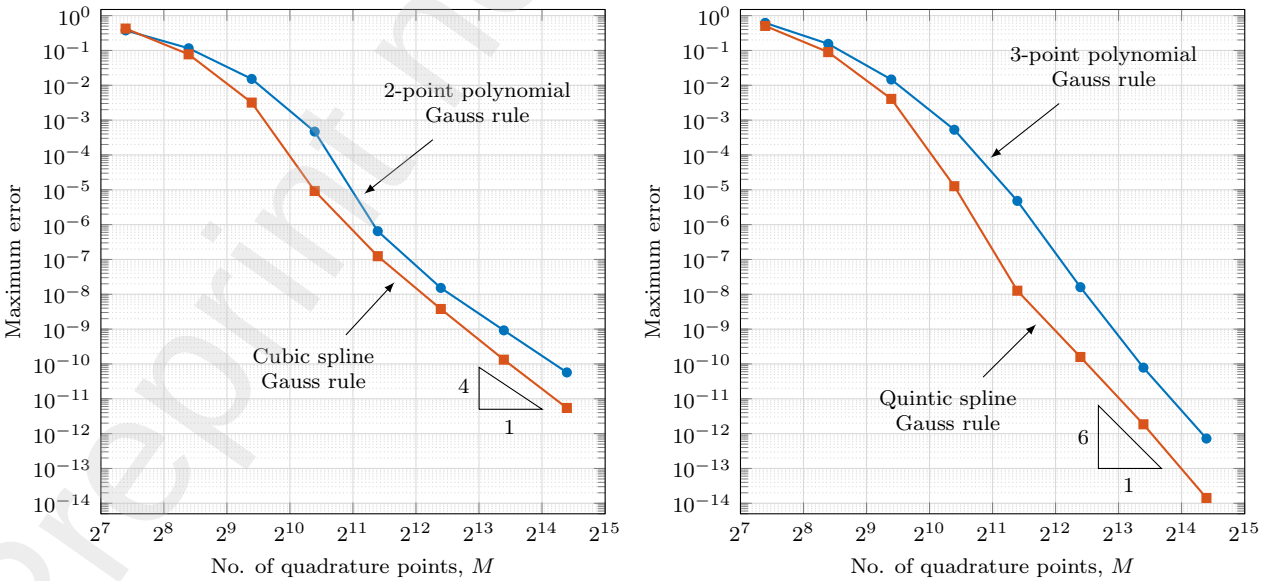

(a) $\widetilde{p} = 3$ (b) $\widetilde{p} = 5$

Fig. 10. Maximum point-wise error of the Nyström approximation of the solution of (5.4) over the unit disk. (a) Cubic spline vs. 2-point polynomial rule. (b) Quintic spline vs. 3-point polynomial rule. The respective numerical convergence orders are shown by the triangles.

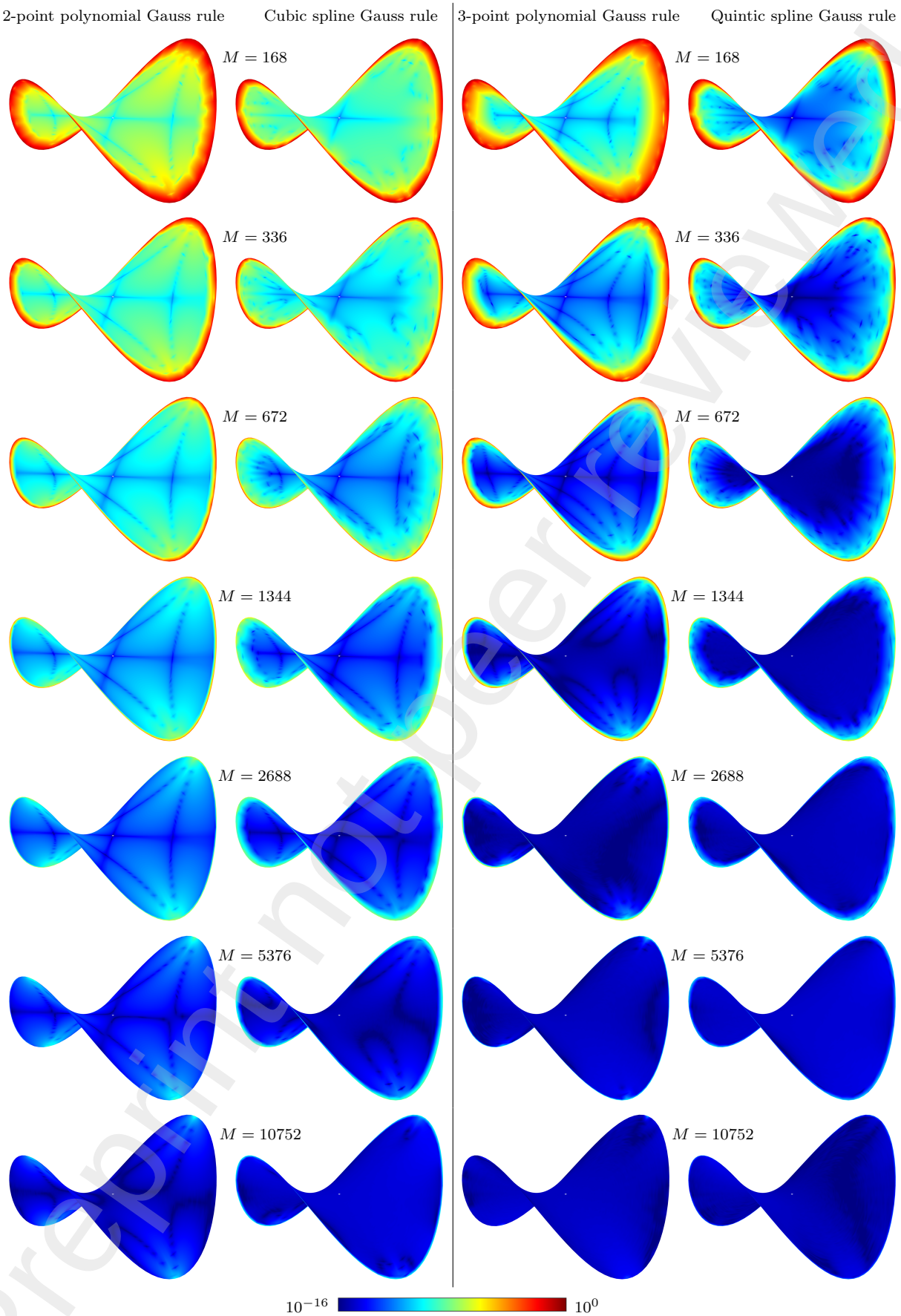

Fig. 11. Error distributions over the unit disk at different refinement levels when comparing 2- and 3-point polynomial Gauss rules with the cubic and quintic spline rules, respectively. We place the error plots over the analytical solution surface.

Fig. 9 shows a NURBS representation of the circular boundary as well as the analytical solution over the domain. We use quadratic basis functions spanned over a knot sequence with double multiplicities at interior knots. Fig. 10 shows the maximum point-wise error of the Nyström approximation of the solution of the Laplace problem (5.4) over a unit disk with a Dirichlet boundary condition. Again, the solutions obtained by the spline Gauss quadrature rules are almost one order of magnitude more accurate compared to their polynomial Gauss counterparts when integrating using the same total number of quadrature points M. The numerical convergence order is also close to the theoretical rate $\widetilde{p}+1$. Fig. 11 illustrates the error distributions over the circular domain when doubling the number of quadrature points at every refinement step. The results well confirm the convergence plots of Fig. 10.

5.3. Steady-state heat transfer analysis inside a blade cascade

The third example is adopted from the fluid flow analysis through turbine blades, which is a well-known practical case study in the computational fluid dynamics (see, e.g., [65–67]). The main idea is to assess the application of the presented methodology in a real-life model problem for which no analytical solution is available. Fig. 12a schematically shows the flow passage through blade cascades of a steam turbine. We simplify the original problem and only consider the steady-state heat transfer inside our computational domain of interest. The heat transfer is governed by the Poisson's equation [68]:

$$-k\nabla^2 T = q\,, \tag{5.6}$$

where T is the fluid temperature, k is the thermal conductivity of the fluid, and q is the rate of heat generation inside the domain. In here, we further assume that no heat source exists, thus, reducing (5.6) to the Laplace equation, i.e., $\nabla^2 T = 0$. We consider Dirichlet boundary conditions as indicated in Fig. 12b and seek to compute the temperature distribution through the blade cascade using the Nyström approximation[1]. In particular, the inlet and outlet temperatures are assumed to be fixed as $T_{\text{in}} = 380°$ and $T_{\text{out}} = 360°$, respectively. While the temperature distribution on the upper and lower parts of the cascade is given by quintic functions with coefficients described in Table 2. We employ a NURBS parameterization of

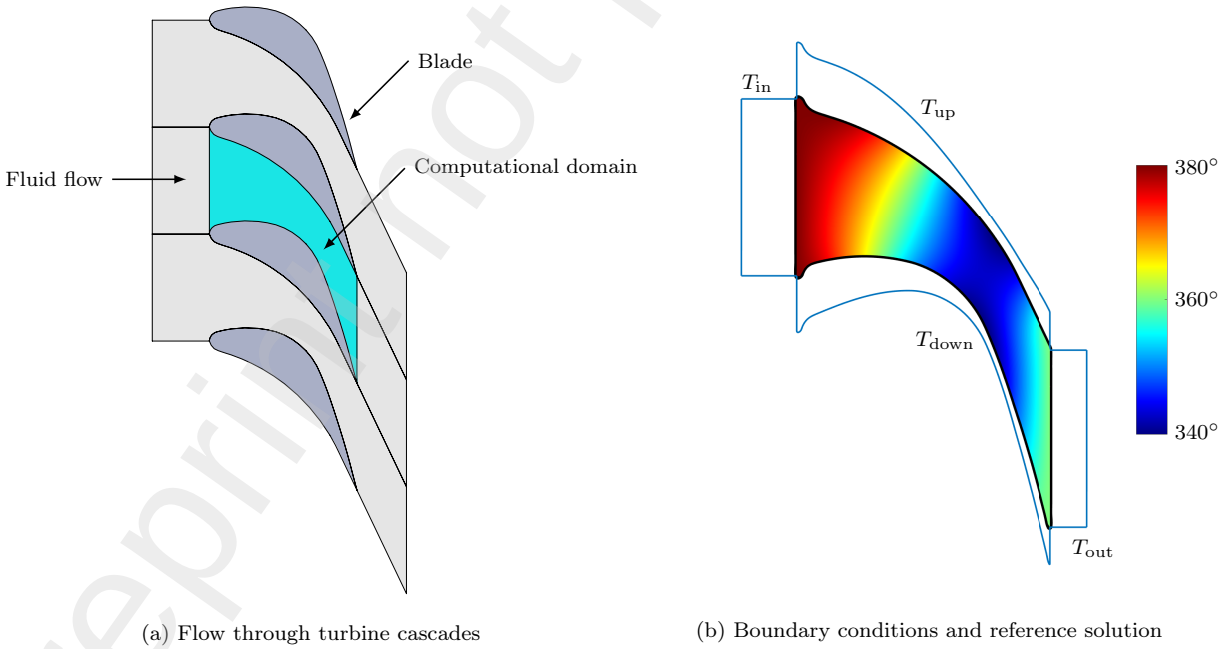

(a) Flow through turbine cascades

(b) Boundary conditions and reference solution

Fig. 12. (a) Schematic view of the fluid flow through blade cascades of a steam turbine. We highlight our computational domain of interest. (b) Dirichlet boundary conditions are overlaid on the four sides of the domain's boundary. We slightly round the corners to reach a better convergence rate in the numerical solution. The reference temperature distribution is color-coded over the domain.

[1] In the original problem, only the inlet temperature is known and the temperature on the other three sides and inside the domain is unknown. It is governed by more parameters such as the pressure, wetness, and turbulence of the fluid.

Table 2. Boundary conditions on different sides of the computational domain of the third example.

Side	Temperature	ξ-range	Coefficients ($\times 10^5$)					
			a_0	a_1	a_2	a_3	a_4	a_5
Up	$T = a_0 + a_1\xi + a_2\xi^2 + a_3\xi^3 + a_4\xi^4 + a_4\xi^5$	[0.15,0.47]	-0.0026	0.1227	-0.9063	3.0780	-4.8648	2.9088
Down		[0.62,1.00]	-0.2985	1.8197	-4.3041	5.0020	-2.8601	0.6446
Inlet	380°							
Outlet	360°							

the boundary and slightly round the sharp corners of the domain to improve the convergence rate of our approximation. Thus, we use the same parameter ξ when imposing boundary conditions T_{up} and T_{down}. Since the analytical solution for this freeform geometry is not available, we obtain the reference temperature distribution using an *overkill* FEA solution with millions of degrees of freedom.

Fig. 13 shows the maximum point-wise error of the Nyström approximation for the third case study. Since the reference solution is also obtained by a numerical method, we observe a plateau in the convergence plots. This is mainly because the accuracy of our solution reaches the accuracy of the reference solution after a few refinement steps. For both cases of $\widetilde{p} = 3$ and 5, the solutions obtained by the spline Gauss quadrature rules are orders of magnitude more accurate than their polynomial Gauss counterparts. Fig. 14 illustrates the error distributions over the computational domain when doubling the number of quadrature points at every refinement step. We observe improvements close to the boundary and, particularly, near the corners when using spline Gauss rules. Nevertheless, for the major interior part of the domain, we can hardly observe significant improvements in error contours, again, because of the numerical nature of our reference solution.

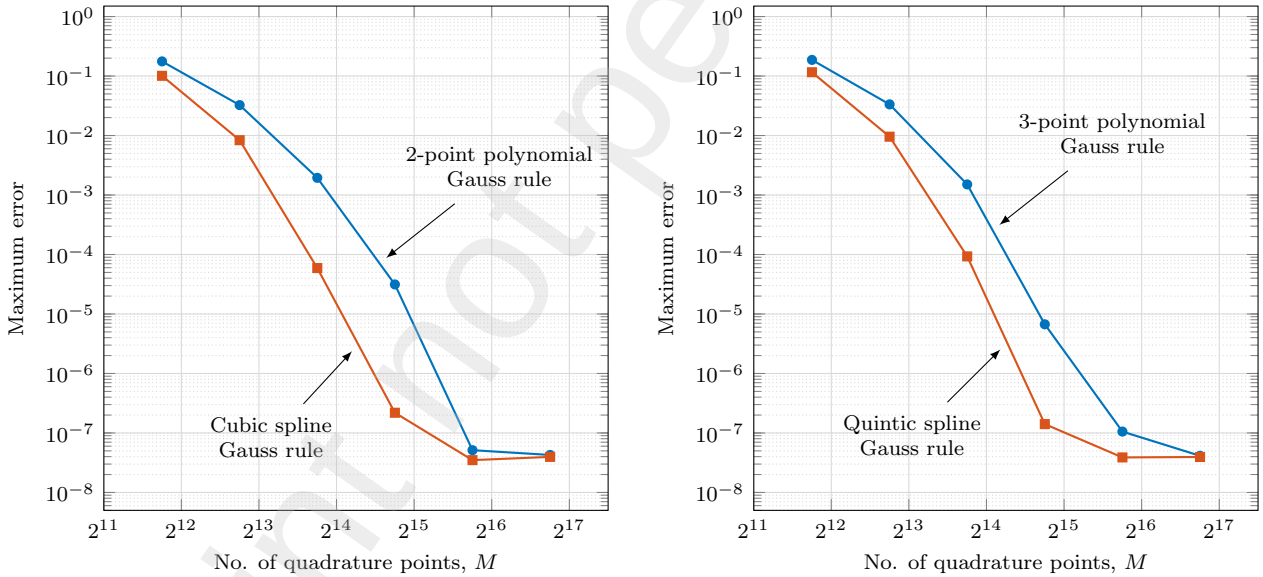

(a) $\widetilde{p} = 3$ (b) $\widetilde{p} = 5$

Fig. 13. Maximum point-wise error of the Nyström approximation of the solution of the third example. (a) Cubic spline vs. 2-point polynomial rule. (b) Quintic spline vs. 3-point polynomial rule. The numerical convergence graphs reach a plateau after a few refinement steps because the reference solution is obtained by FEA, which is a numerical method as well.

6. Conclusions

We propose to use spline Gauss quadrature rules for solving boundary value problems using the Nyström method. The corresponding PDE inside a domain is converted into the Fredholm integral equation of the second kind on the boundary. Then, we use spline Gauss quadratures and convert the integral equation to a linear system via the Nyström method. We consider the solution of the Laplace equation in 2D domains when Dirichlet boundary conditions are applied. We validate our method on three different geometries,

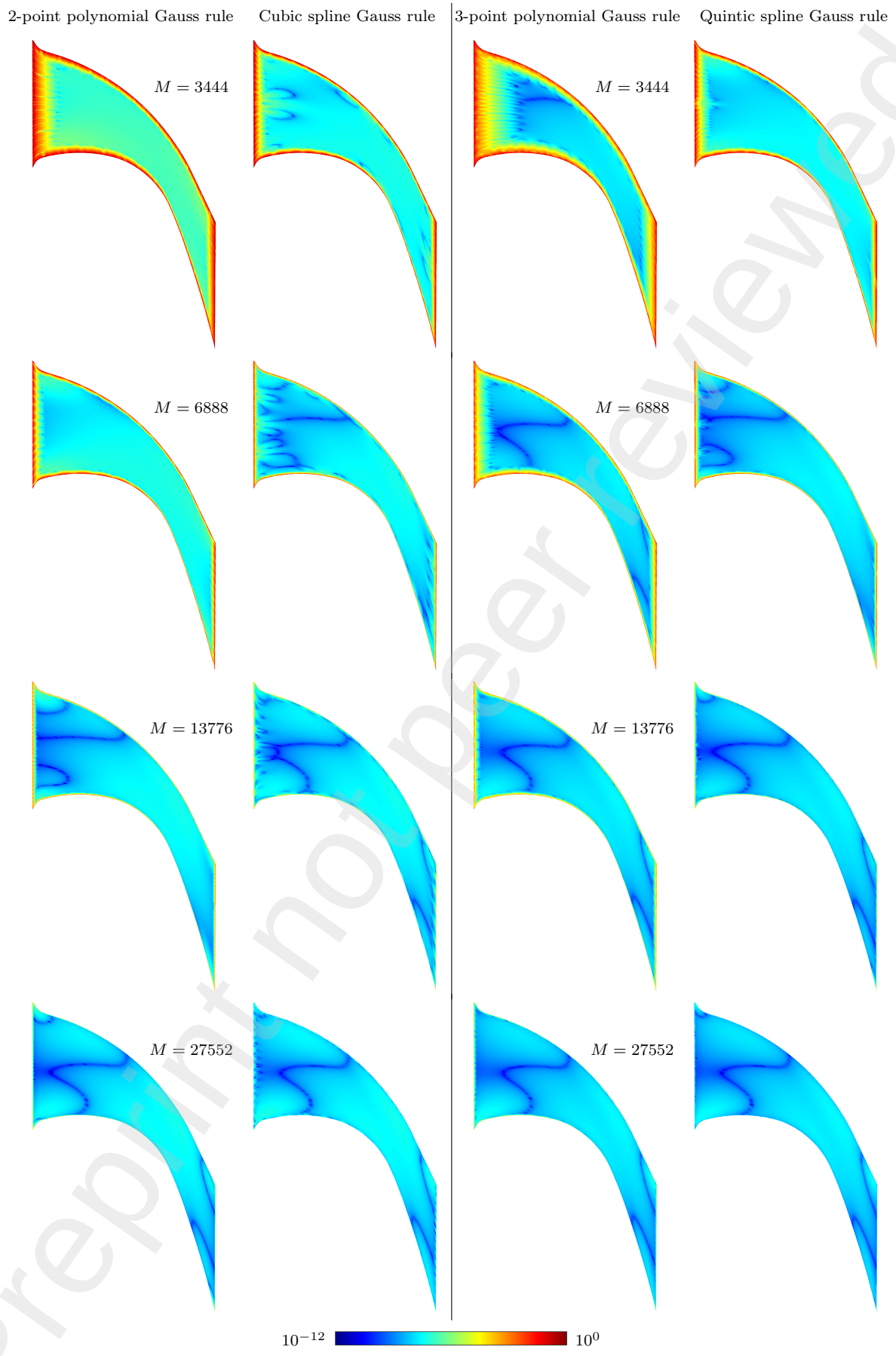

Fig. 14. Error distributions through the blade cascade of the third example. We compare 2- and 3-point polynomial Gauss rules with the cubic and quintic spline rules, respectively, when doubling the total number of quadrature points.

namely: square, circular, and freeform domains. When using a NURBS representation of the boundary, we place the quadrature points within the knot spans of the NURBS geometry. In this context, we compare the macroelement-wise integration of the spline Gauss rules with the element-wise integration of the polynomial Gauss rules. The results indicate that, when fixing the total number of quadrature points (i.e., with the same computational effort), the spline rules return an approximation that is by one to two orders of magnitude more accurate compared to the solution obtained by traditional polynomial Gauss counterparts.

As future work, we aim to consider a non-uniform refinement in terms of non-uniform Gaussian spline rules, which are expected to capture better the features of more complicated boundary curves, and possibly further reduce the approximation error.

Acknowledgment

This work has received funding from the Spanish Ministry of Science and Innovation projects with references PID2019-108111RB-I00 and PID2019-104488RB-I00, the "BCAM Severo Ochoa" accreditation of excellence (SEV-2017-0718) and the Basque Government through the BERC 2022-2025 program. The third author is a member of the INdAM-GNCS Research group. The fourth author is a member of the IMAG, the Institute of Mathematics of the University of Granada.

References

[1] W. Hackbusch, Integral Equations: Theory and Numerical Treatment, Birkhäuser Basel, Switzerland, 1995.
[2] G. Beer, I. Smith, C. Duenser, The Boundary Element Method with Programming, Springer-Verlag, New York, NY, 2008.
[3] K. Atkinson, W. Han, Theoretical Numerical Analysis: A Functional Analysis Framework, Springer, New York, NY, 2009. doi:10.1007/978-1-4419-0458-4.
[4] J. N. Reddy, An Introduction to the Finite Element Method, 4th Edition, McGraw-Hill, New York, NY, 2018.
[5] J. A. Cottrell, T. J. R. Hughes, Y. Bazilevs, Isogeometric Analysis: Toward Integration of CAD and FEA, John Wiley & Sons, Ltd, New York, NY, 2009.
[6] K. Atkinson, A. Bogomolny, The discrete Galerkin method for integral equations, Mathematics of Computation 48 (178) (1987) 595. doi:10.2307/2007830.
[7] S. Joe, Discrete Galerkin methods for Fredholm integral equations of the second kind, IMA Journal of Numerical Analysis 7 (2) (1987) 149–164. doi:10.1093/imanum/7.2.149.
[8] S. Joe, Discrete collocation methods for second kind Fredholm integral equations, SIAM Journal on Numerical Analysis 22 (6) (1985) 1167–1177. doi:10.1137/0722070.
[9] E. N. Houstis, T. S. Papatheodorou, A collocation method for Fredholm integral equations of the second kind, Mathematics of Computation 32 (141) (1978) 159–173. doi:10.1090/s0025-5718-1978-0458967-8.
[10] H. Esmaeili, F. Mirzaee, D. Moazami, A discrete collocation scheme to solve Fredholm integral equations of the second kind in high dimensions using radial kernels, SeMA Journal 78 (1) (2021) 93 – 117. doi:10.1007/s40324-020-00231-0.
[11] M. Wang, Multistep collocation method for Fredholm integral equations of the second kind, Applied Mathematics and Computation 420 (2022) 126870. doi:10.1016/j.amc.2021.126870.
[12] G. Beer, J. Watson, Introduction to Finite and Boundary Element Methods for Engineers, Wiley, New York, NY, 1992.
[13] W. L. Wendland, Boundary Element Topics, Springer, Berlin, Germany, 1997.
[14] A. Aimi, M. Diligenti, M. L. Sampoli, A. Sestini, Isogemetric analysis and symmetric Galerkin BEM: A 2D numerical study, Applied Mathematics and Computation 272 (2016) 173–186. doi:10.1016/j.amc.2015.08.097.
[15] K. V. Kostas, M. M. Fyrillas, C. G. Politis, A. I. Ginnis, P. D. Kaklis, Shape optimization of conductive-media interfaces using an IGA-BEM solver, Computer Methods in Applied Mechanics and Engineering 340 (2018) 600–614. doi:10.1016/j.cma.2018.06.019.
[16] A. Aimi, F. Calabrò, M. Diligenti, M. L. Sampoli, G. Sangalli, A. Sestini, Efficient assembly based on B-spline tailored quadrature rules for the IgA-SGBEM, Computer Methods in Applied Mechanics and Engineering 331 (2018) 327–342. doi:10.1016/j.cma.2017.11.031.
[17] A. Falini, C. Giannelli, T. Kanduč, M. L. Sampoli, A. Sestini, An adaptive IgA-BEM with hierarchical B-splines based on quasi-interpolation quadrature schemes, International Journal for Numerical Methods in Engineering 117 (10) (2019) 1038–1058. doi:10.1002/nme.5990.
[18] G. Beer, B. Marussig, C. Duenser, The Isogeometric Boundary Element Method, Springer International Publishing, Switzerland, 2020.
[19] I. H. Sloan, B. J. Burn, N. Datyner, A new approach to the numerical solution of integral equations, Journal of Computational Physics 18 (1) (1975) 92–105. doi:10.1016/0021-9991(75)90104-7.
[20] I. H. Sloan, Error analysis for a class of degenerate-kernel methods, Numerische Mathematik 25 (3) (1975) 231–238. doi:10.1007/bf01399412.
[21] C. Allouch, P. Sablonnière, D. Sbibih, Solving Fredholm integral equations by approximating kernels by spline quasi-interpolants, Numerical Algorithms 56 (3) (2011) 437 – 453. doi:10.1007/s11075-010-9396-7.
[22] D. Barrera, F. Elmokhtari, D. Sbibih, Two methods based on bivariate spline quasi-interpolants for solving Fredholm integral equations, Applied Numerical Mathematics 127 (2018) 78 – 94. doi:10.1016/j.apnum.2017.12.016.
[23] D. Barrera, F. El Mokhtari, M. J. I. nez, D. Sbibih, Non-uniform quasi-interpolation for solving Hammerstein integral equations, International Journal of Computer Mathematics 97 (1-2) (2020) 72 – 84. doi:10.1080/00207160.2018.1435867.
[24] C. Allouch, S. Remogna, D. Sbibih, M. Tahrichi, Superconvergent methods based on quasi-interpolating operators for Fredholm integral equations of the second kind, Applied Mathematics and Computation 404 (2021) 126227. doi:10.1016/j.amc.2021.126227.

[25] C. Dagnino, A. Dallefrate, S. Remogna, Spline quasi-interpolating projectors for the solution of nonlinear integral equations, Journal of Computational and Applied Mathematics 354 (2019) 360 – 372. doi:10.1016/j.cam.2018.06.054.
[26] D. Barrera, F. El Mokhtari, M. J. I. nez, D. Sbibih, A quasi-interpolation product integration based method for solving Love's integral equation with a very small parameter, Mathematics and Computers in Simulation 172 (2020) 213 – 223. doi:10.1016/j.matcom.2019.12.008.
[27] C. Dagnino, S. Remogna, P. Sablonnière, On the solution of Fredholm integral equations based on spline quasi-interpolating projectors, BIT Numerical Mathematics 54 (4) (2014) 979–1008. doi:10.1007/s10543-014-0486-0.
[28] E. J. Nyström, Über die praktische auflösung von linearen integralgleichungen mit anwendungen auf randwertaufgaben der potentialtheorie, Societas scientiarum Fennica Commentationes Physico-Mathematicae 4 (1928) 1 – 52.
[29] E. J. Nyström, Über die praktische auflösung von integralgleichungen mit anwendungen auf randwertaufgaben, Acta Mathematica 54 (1930) 185 – 204. doi:10.1007/BF02547521.
[30] A. Kirsch, P. Monk, An analysis of the coupling of finite-element and Nyström methods in acoustic scattering, IMA Journal of Numerical Analysis 14 (4) (1994) 523–544. doi:10.1093/imanum/14.4.523.
[31] A. Anand, J. S. Ovall, S. Weißer, A Nyström-based finite element method on polygonal elements, Computers & Mathematics with Applications 75 (11) (2018) 3971–3986. doi:10.1016/j.camwa.2018.03.007.
[32] J. Zechner, B. Marussig, G. Beer, T.-P. Fries, The isogeometric Nyström method, Computer Methods in Applied Mechanics and Engineering 308 (2016) 212–237. doi:10.1016/j.cma.2016.03.043.
[33] Z. Liu, M. Yang, J. Cheng, D. Wu, J. Tan, Meta-model based stochastic isogeometric analysis of composite plates, International Journal of Mechanical Sciences 194 (2021) 106194. doi:10.1016/j.ijmecsci.2020.106194.
[34] Z. G. Zhou, Y. J. Zhang, R. X. Gao, M. S. Tong, A higher-order Nyström discretization of surface integral equations for electromagnetic scattering by penetrable objects, in: 2018 IEEE International Symposium on Antennas and Propagation & USNC/URSI National Radio Science Meeting, IEEE, 2018. doi:10.1109/apusncursinrsm.2018.8609057.
[35] M. S. Tong, W. C. Chew, The Nystrom Method in Electromagnetics, John Wiley & Sons, Hoboken, NJ, 2020.
[36] R. Chen, S. B. Sayed, H. A. Ulku, H. Bagci, An explicit time marching scheme for efficient solution of the magnetic field integral equation at low frequencies, IEEE Transactions on Antennas and Propagation 69 (2) (2021) 1213–1218. doi:10.1109/tap.2020.3010997.
[37] B. Wu, H. Zhu, A. Barnett, S. Veerapaneni, Solution of Stokes flow in complex nonsmooth 2D geometries via a linear-scaling high-order adaptive integral equation scheme, Journal of Computational Physics 410 (2020) 109361. doi:10.1016/j.jcp.2020.109361.
[38] L. Bystricky, S. Pålsson, A.-K. Tornberg, An accurate integral equation method for Stokes flow with piecewise smooth boundaries, BIT Numerical Mathematics 61 (1) (2020) 309–335. doi:10.1007/s10543-020-00816-1.
[39] W. Wang, G. Chen, D. Yang, Z. Kang, Stochastic isogeometric analysis method for plate structures with random uncertainty, Computer Aided Geometric Design 74 (2019) 101772. doi:10.1016/j.cagd.2019.101772.
[40] Z. Liu, M. Yang, J. Cheng, D. Wu, J. Tan, Stochastic isogeometric analysis for the linear stability assessment of plate structures using a Kriging enhanced neural network, Thin-Walled Structures 157 (2020) 107120. doi:10.1016/j.tws.2020.107120.
[41] S. Hao, A. H. Barnett, P. G. Martinsson, P. Young, High-order accurate methods for Nyström discretization of integral equations on smooth curves in the plane, Advances in Computational Mathematics 40 (1) (2014) 245–272. doi:10.1007/s10444-013-9306-3.
[42] M. Bartoň, V. M. Calo, Gaussian quadrature for splines via homotopy continuation: Rules for C^2 cubic splines, Journal of Computational and Applied Mathematics 296 (2016) 709–723. doi:10.1016/j.cam.2015.09.036.
[43] M. Bartoň, V. M. Calo, Optimal quadrature rules for odd-degree spline spaces and their application to tensor-product-based isogeometric analysis, Computer Methods in Applied Mechanics and Engineering 305 (2016) 217–240. doi:10.1016/j.cma.2016.02.034.
[44] R. Kress, Linear Integral Equations, Springer Berlin Heidelberg, Germany, 1989.
[45] K. Atkinson, The Numerical Solution of Integral Equations of the Second Kind, Cambridge University Press, Cambridge, UK, 1997. doi:10.1017/CBO9780511626340.
[46] I. J. Schoenberg, Spline functions, convex curves and mechanical quadrature, Bulletin of the American Mathematical Society 64 (6) (1958) 352–357. doi:10.1090/S0002-9904-1958-10227-X.
[47] P. J. Davis, P. Rabinowitz, Methods of Numerical Integration, 2nd Edition, Academic Press, Inc.,, Orlando, FL, 1984. doi:10.1016/C2013-0-10566-1.
[48] J. Strain, Locally corrected multidimensional quadrature rules for singular functions, SIAM Journal on Scientific Computing 16 (4) (1995) 992–1017. doi:10.1137/0916058.
[49] L. F. Canino, J. J. Ottusch, M. A. Stalzer, J. L. Visher, S. M. Wandzura, Numerical solution of the Helmholtz equation in 2D and 3D using a high-order Nyström discretization, Journal of Computational Physics 146 (2) (1998) 627–663. doi:10.1006/jcph.1998.6077.
[50] L. Piegl, W. Tiller, The NURBS Book, 2nd Edition, Springer-Verlag, New York, NY, 1997.
[51] A. Hashemian, D. Garcia, D. Pardo, V. M. Calo, Refined isogeometric analysis of quadratic eigenvalue problems, Computer Methods in Applied Mechanics and Engineering 399 (2022) 115327. doi:10.1016/j.cma.2022.115327.
[52] W. Gautschi, Numerical Analysis, Birkhäuser, Boston, MA, 2012.
[53] S. Karlin, W. J. Studden, Tchebycheff systems: With applications in analysis and statistics, SIAM Review 9 (2) (1967) 257–258. doi:10.1137/1009050.
[54] C. A. Micchelli, A. Pinkus, Moment theory for weak chebyshev systems with applications to monosplines, quadrature formulae and best one-sided l^1-approximation by spline functions with fixed knots, SIAM Journal on Mathematical Analysis 8 (2) (1977) 206–230. doi:10.1137/0508015.
[55] T. J. R. Hughes, A. Reali, G. Sangalli, Efficient quadrature for NURBS-based isogeometric analysis, Computer Methods in Applied Mechanics and Engineering 199 (5) (2010) 301–313. doi:10.1016/j.cma.2008.12.004.
[56] A. J. Sommese, C. W. Wampler, The Numerical Solution of Systems of Polynomials Arising in Engineering and Science, World Scientific, Singapore, 2005.
[57] M. Bartoň, V. M. Calo, Gauss–Galerkin quadrature rules for quadratic and cubic spline spaces and their application to isogeometric analysis, Computer-Aided Design 82 (2017) 57–67. doi:10.1016/j.cad.2016.07.003.
[58] D. Barrera, M. Bartoň, I. Chiarella, S. Remogna, On numerical solution of Fredholm and Hammerstein integral equations via Nyström method and Gaussian quadrature rules for splines, Applied Numerical Mathematics 174 (2022) 71–88. doi:10.1016/j.apnum.2022.01.009.
[59] M. Bartoň, R. Ait-Haddou, V. M. Calo, Gaussian quadrature rules for C^1 quintic splines with uniform knot vectors,

Journal of Computational and Applied Mathematics 322 (2017) 57–70. doi:10.1016/j.cam.2017.02.022.
[60] R. Kress, A Nyström method for boundary integral equations in domains with corners, Numerische Mathematik 58 (1) (1990) 145–161. doi:10.1007/bf01385616.
[61] A. Gillman, S. Hao, P. G. Martinsson, A simplified technique for the efficient and highly accurate discretization of boundary integral equations in 2D on domains with corners, Journal of Computational Physics 256 (2014) 214–219. doi:10.1016/j.jcp.2013.08.049.
[62] G. J. Wagner, W. K. Liu, Hierarchical enrichment for bridging scales and mesh-free boundary conditions, International Journal for Numerical Methods in Engineering 50 (3) (2001) 507–524. doi:10.1002/1097-0207(20010130)50:3<507::aid-nme33>3.0.co;2-b.
[63] A. Embar, J. Dolbow, I. Harari, Imposing Dirichlet boundary conditions with Nitsche's method and spline-based finite elements, International Journal for Numerical Methods in Engineering 83 (7) (2010) 877–898. doi:10.1002/nme.2863.
[64] J. Lebl, Dirichlet problem in the circle and the Poisson kernel, in: Differential Equations for Engineers, LibreTexts, Stillwater, OK, 2022.
[65] A. Hashemian, E. Lakzian, A. Ebrahimi-Fizik, On the application of isogeometric finite volume method in numerical analysis of wet-steam flow through turbine cascades, Computers & Mathematics with Applications 79 (6) (2020) 1687–1705. doi:10.1016/j.camwa.2019.09.025.
[66] Y. Patel, G. Patel, T. Turunen-Saaresti, Influence of turbulence modelling on non-equilibrium condensing flows in nozzle and turbine cascade, International Journal of Heat and Mass Transfer 88 (2015) 165–180. doi:10.1016/j.ijheatmasstransfer.2015.04.069.
[67] D. Hoseinzade, E. Lakzian, A. Hashemian, A blackbox optimization of volumetric heating rate for reducing the wetness of the steam flow through turbine blades, Energy 220 (2021) 119751. doi:10.1016/j.energy.2020.119751.
[68] L. C. Evans, Partial Differential Equations, 2nd Edition, American Mathematical Society, Providence, RI, 2010.